Asian Journal of Chemistry; Vol. 37, No. 8 (2025), 2059-2071

ASIAN JOURNAL OF CHEMISTRY

https://doi.org/10.14233/ajchem.2025.33983

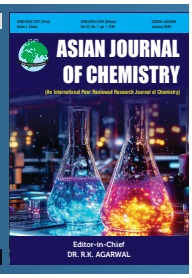

Synthesis, Spectroscopic Characterization (FT-IR, FT-Raman and NMR) and *in vitro* Anticancer Activity of (*E*)-5-Bromo-3-((4-chloro-3-(trifluoromethyl)phenyl)imino)indolin-2-one

S. Rekha[1,*], S. Tamilselvan[1,*], Malik Nasibullah[2], Mohd Asif[2], P. Manikandan[1], V.S. Jeba Reeda[3] and S. Kaleeswaran[4]

[1]Department of Physics, Arignar Anna Government Arts College, Cheyyar-604407, India
[2]Medicinal Chemistry Laboratory-ICEIR, Department of Chemistry, Integral University, Lucknow-226026, India
[3]Department of Physics, Easwari Engineering College, Ramapuram, Chennai-600089, India
[4]Department of Physics, Madras Christian College, East Tambaram, Chennai-600059, India

*Corresponding authors: E-mail: rekhasowri@gmail.com; tamilraji1977@gmail.com

Received: 5 May 2025; *Accepted*: 19 July 2025; *Published online*: 31 July 2025; AJC-22086

This comprehensive study, combining theoretical insights with experimental validation, enhances the understanding of molecular structure, vibrational dynamics and electron delocalization through spectroscopic techniques. These methods were employed to analyze the synthesized hybrid oxindole Schiff base, specifically (*E*)-5-bromo-3-((4-chloro-(trifluoromethyl)phenyl)imino)indolin-2-one (5BTPIO) molecule, as well as its biological activities. Electron localization function (ELF), localized orbital locator (LOL) and reduced density gradient (RDG) investigations facilitated to classify the weakest interactions, bonding zones and electron energy density, respectively. The *in vitro* anticancer properties of the 5BTPIO molecule were also investigated. The *in silico* docking studies were executed to preliminarily assess the anticancer activity against 3G74, 4Z8Z and 7PGL proteins, revealing binding affinities of -6.08, -5.60 and -6.72 kcal/mol, respectively. DFT proved valuable in examining the stability of the molecular structure under optimal conditions, facilitating comparison studies that integrated both theoretical and experimental data.

Keywords: Hybrid oxindole, DFT, Docking studies, Anticancer activity.

INTRODUCTION

Nowadays, cancer is one of the most challenging illnesses to eradicate in humans. According to WHO, 9.7 to 10 million people passed away as a result of uncontrolled growth of cells in living organisms, which led to the development of various cancers [1,2]. However, the discovery of new drug is needed that could be inhibited to the uncontrolled growing cancer cells through the chemotherapy treatment. That was noted from the literature reports that interactions amongst the targeted amino acid residues of the proteins, the imine activities of the Schiff bases have become fascinating in medicinal chemistry [3-6]. Many carcinomas have been treated with compounds containing functionalized imines and the FDA has approved these drug-like compounds [7,8]. Conversely, previous studies have successfully employed imine-containing oxindole small molecules in cancer treatment [9,10]. Based on these findings, we chose to synthesize a functionalized hybrid oxindole-imine small molecule [(*E*)-5-bromo-3-((4-chloro-3-(trifluoromethyl)-phenyl)imino)indolin-2-one] as an effective anticancer agent. Several spectroscopic techniques were used to characterize the synthesized hybrid oxindole-Schiff base.

Furthermore, density functional theory (DFT) was utilized to evaluate these spectra to govern the structure of synthesized molecule. The *in silico* analysis of the synthesized molecule was assessed by the National Cancer Institute (NCI) for its efficacy against sixty distinct human cancer cell lines through laboratory experiments (*in vitro* assays). Its electronic stability was evaluated using (NBO) analysis, along with LOL, RDG and ELF studies. Molecular docking experiments showed how the compound binds to target proteins. Overall, the compound demonstrated good drug-likeness, favourable ADMET properties strong docking affinity and significant anticancer activity. This makes it a promising lead candidate for cancer treatment.

Further structural modifications could improve its effectiveness.

EXPERIMENTAL

Characterization: The melting point was determined using an open capillary method with a Griffin IA 9100 MK-Digital instrument. Infrared (IR) spectra were recorded with Agilent Cary 630 FT-IR spectrometer, in the range of 4000 to 450 cm^{-1}. NMR were measured in DMSO on a Bruker Avance 400 MHz instrument for hydrogen (^{1}H) and a Bruker AVII 100 MHz for carbon (^{13}C), with TMS serving as internal reference. FT-Raman spectroscopy was conducted with a Bruker RFS 27 laser (1064 nm wavelength) instrument having a resolution of 2 cm^{-1} across the 4000 to 100 cm^{-1} range.

Synthesis: 5-Bromo dioxindole and 4-chloro-3-(trifluoromethyl)aniline were refluxed in ethanol for 21 min to obtain (*E*)-5-bromo-3-((4-chloro-3-(trifluoromethyl)phenyl)imino)-indolin-2-one (5BTPIO) in the presence of fluoroacetic acid (1 g) as catalyst and stirred the reaction mixture at ambient temperature. Following the formation of a crude yellow precipitate, pure component was separated using column chromatography and purified with ethyl acetate and *n*-hexane (**Scheme-I**).

Computational details: Gaussian 09W [11] and Gauss view 5.0 [12] have been utilized to compute the optimal structure employing B3LYP/6-311++G(d,p) [13]. The chemical's PED were standardized as part of the vibrational investigation using VEDA software [14] and the scaling factor is 0.961 [15]. Using the Chemcraft tool [16], Bond lengths and angles were determined following the structural optimization. NBO analysis revealed interactions between lone pairs and both bonding and anti-bonding orbitals [17]. For the topological analyses and electron excitation, the Multiwave function analysis [18] program was utilized. Investigations on the pharmacological properties and lipophilicity was carried out through the SwissADME online program [19]. PatchDock Tools was used to accomplish the molecular docking analysis [20].

RESULTS AND DISCUSSION

Geometry optimization: Fig. 1 shows the theoretically computed optimum structure of (*E*)-5-bromo-3-((4-chloro-3-(trifluoromethyl)phenyl)imino)indolin-2-one (5BTPIO), while Table-1 highlights the computed values. A thorough assessment indicates that no observable or theoretical study on the title compound was conducted. There are 32 bond lengths and 52 bond angles in the aforementioned compound. Due to the homonuclearity, the bond length at C6-Br23 = 1.915 Å is larger. The maximum bond lengths between C15 and Cl22 were measured (1.749 Å) and these bonds may possess greater value. In contrast, the bond distance of N1-H24 is less (1.009 Å). C4-C3-N11 had the largest bond angle value (134.5), while N1-C2-C3 had the lowest bond angle value (104.9).

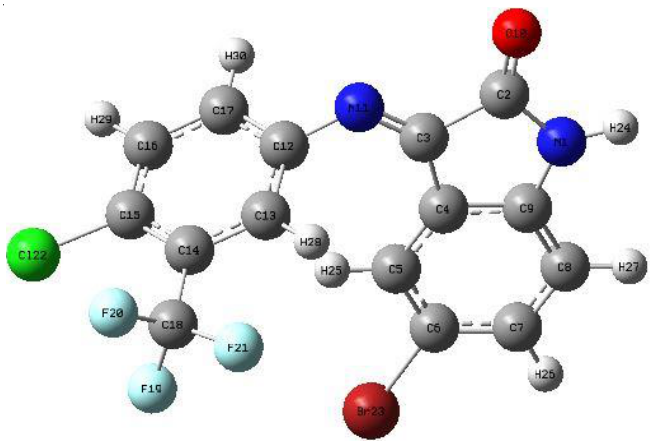

Fig. 1. Optimized structure of 5BTPIO molecule

Vibrational analysis: The vibrational spectroscopy was utilized to identify distinct functional groups within the molecule [21]. The vibrational assignments applied in the VEDA program, with a scaling factor of 0.961, enhanced the agreement between the experimental and computational results with the infrared spectra of the 5BTPIO molecule. Given that the molecule under investigation has 30 atoms, there are 84 normal vibrational modes. Calculated vibrational wave counts and associated PED are shown in Table-2. Fig. 2 displays the FTIR and Raman experimental spectra.

C–C vibrations: In 1650-1200 cm^{-1} range, the vibrations related to C–C stretching are very evident [22]. At 1614 and 1328 cm^{-1}, C–C vibrations were detected at 1551 and 1276 cm^{-1}, a scaled value with PEDs of 50, 27 and 16% was observed. The experimental FT-IR bonds are 1600 and 1300 cm^{-1}, while the experimental Raman band has a good significant peak at 1616 and 1750 cm^{-1}.

O-C vibrations: The primary vibration of CO typically occurs within the range of 1850 to 1550 cm^{-1} [23]. The 5BTPIO vibrations were detected at 1736 cm^{-1} and 1749 cm^{-1} in both

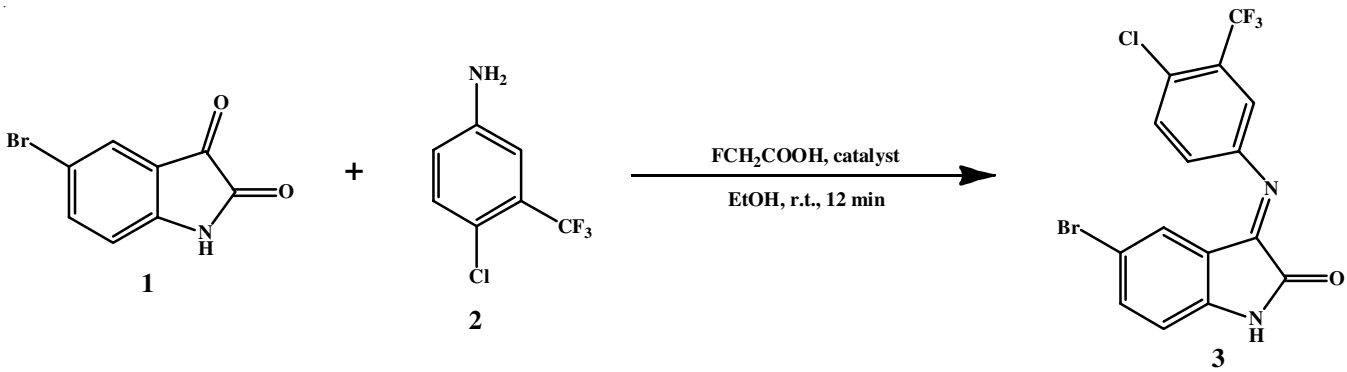

Scheme-I: Synthesis of (E)-5-bromo-3-((4-chloro-3-(trifluoromethyl)phenyl)imino)indolin-2-one (5BTPIO)

TABLE-1
OPTIMIZED GEOMETRICAL PARAMETERS OF 5BTPIO MOLECULE

Bond length (Å)	B3LYP/6-311++ G(d,p)	Bond angle (°)	B3LYP/6-311++G(d,p)	Bond angle (°)	B3LYP/6-311++G(d,p)
N1-C2	1.387	C2-N1-C9	112.2	C7-C8-H27	120.3
N1-C9	1.397	C2-N1-H24	122.3	C9-C8-H27	121.6
N1-H24	1.009	N1-C2-C3	104.9	N11-C12-C13	120.8
C2-C3	1.542	N1-C2-O10	126.7	N11-C12-C17	119.8
C2-O10	1.204	C9-N1-H24	125.4	C13-C12-C17	119.1
C3-C4	1.475	N1-C9-C4	110.1	C12-C13-C14	121.0
C3-N11	1.269	N1-C9-C8	128.5	C12-C13-H28	119.5
C4-C5	1.392	C3-C2-O10	128.4	C12-C17-C16	120.0
C4-C9	1.41	C2-C3-C4	105.7	C12-C17-H30	120.0
C5-C6	1.395	C2-C3-N11	119.7	C14-C13-H28	119.5
C5-H25	1.079	C4-C3-N11	134.5	C13-C14-C15	119.3
C6-C7	1.394	C3-C4-C5	132.7	C13-C14-C18	118.8
C6-Br23	1.915	C3-C4-C9	107.0	C15-C14-C18	122.0
C7-C8	1.398	C3-N11-C12	122.8	C14-C15-C16	119.8
C7-H26	1.083	C5-C4-C9	120.2	C14-C15-Cl22	122.2
C8-C9	1.386	C4-C5-C6	118.2	C14-C18-F19	111.8
C8-H27	1.083	C4-C5-H25	121.3	C14-C18-F20	112.3
N11-C12	1.407	C4-C9-C8	121.4	C14-C18-F21	111.6
C12-C13	1.4	C6-C5-H25	120.5	C16-C15-Cl22	118.1
C12-C17	1.4	C5-C6-C7	121.4	C15-C16-C17	120.8
C13-C14	1.394	C5-C6-Br23	119.2	C15-C16-H29	119.2
C13-H28	1.081	C7-C6-Br23	119.4	C17-C16-H29	120.0
C14-C15	1.403	C6-C7-C8	120.6	C16-C17-H30	120.0
C14-C18	1.513	C6-C7-H26	119.8	F19-C18-F20	107.4
C15-C16	1.393	C8-C7-H26	119.6	F19-C18-F21	106.5
C15-Cl22	1.749	C7-C8-C9	118.1	F20-C18-F21	106.8
C16-C17	1.389				
C16-H29	1.083				
C17-H30	1.083				
C18-F19	1.356				
C18-F20	1.346				
C18-F21	1.351				

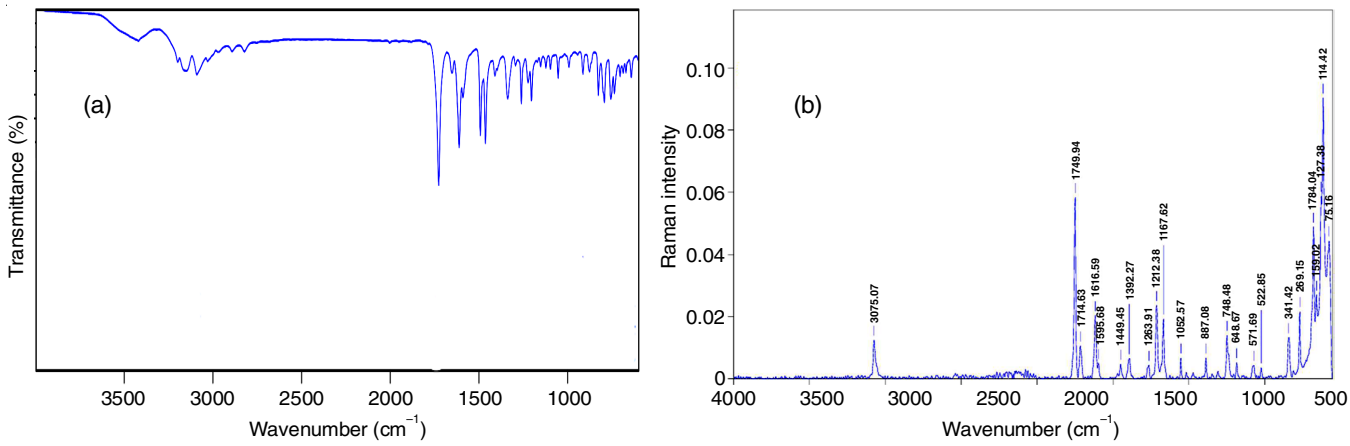

Fig. 2. Experimental spectra of (a) FT-IR and (b) FT-Raman of 5BTPIO molecule

experimental IR and Raman analyses. Theoretical calculations of CO stretching suggest a value of 1756 cm^{-1}, accounting for 84% of PED.

C–H vibrations: The C–H symmetric vibrations typically occur between 3300 and 3000 cm^{-1} [24]. In current study, Raman at 3075 cm^{-1} and FTIR experiment value at 3070 cm^{-1} were identified as strong and weak peaks, respectively. Theoretical C-H vibrations with 99 and 100% PED unscaled value were observed at 3228, 3188 and 3185 cm^{-1} and scaled values were observed at 3102 and 3060 cm^{-1}. All the computed wavenumbers for 5BTPIO fell within the predicted range.

C–N vibration: Identifying the C–N stretching frequency in the side chains can be tricky because it often overlaps with other vibrations. Kahovec & Kohlrausch [25] reported the C=N stretching vibration in salicylic aldoxime at 1617 cm^{-1}. In our study, the computed C=N vibration appears at 1658 cm^{-1}. Experimentally, the values around 1631 cm^{-1} in IR spectra and 1616 cm^{-1} in Raman spectra were observed.

TABLE-2
VIBRATIONAL ASSIGNMENT OF 5BPFIO MOLECULE

Modes	Experimental		B3LYP/6-311++G(P,D)		IR Intensity		Raman Intensity		[d]PED (%)
	IR	Raman	Unscaled	Scaled	[b]Relative	Absolute	[c]Relative	Absolute	
84			3640	3498	80	17	228	16	γNH (100)
83	3166		3228	3102	1	0	40	3	γCH (99)
82	3110		3215	3089	2	0	43	3	γCH (99)
81			3207	3082	1	0	146	10	γCH (99)
80		3075	3205	3080	1	0	171	12	γCH (100)
79	2841		3192	3068	1	0	53	4	γCH (100)
78			3185	3060	6	1	129	9	γCH (100)
77	1736	1749	1827	1756	482	100	77	6	γOC (84)
76	1631	1616	1726	1658	131	27	1398	100	γNC (79)
75		1595	1648	1583	162	34	228	16	γCC (56)
74			1628	1565	19	4	584	42	γCC (67) + βHCC (10)
73			1614	1551	0	0	20	1	γCC (50)
72	1500		1597	1534	5	1	105	7	γCC (48) + βCCC (14)
71	1498	1449	1502	1444	60	12	2	0	βHCC (46)
70			1489	1431	158	33	43	3	βHCC (57)
69			1462	1405	84	18	12	1	γCC (52)
68		1392	1432	1376	70	15	10	1	γCC (40) + βHCC (19)
67	1332		1403	1348	38	8	91	6	γCC (11) + βHCC (19) + γNC (14) + βHCC (33)
66			1328	1276	182	38	84	6	γCC (16) + γCC (27)
65		1263	1307	1256	117	24	25	2	βHCC (31)
64	1249		1301	1250	19	4	3	0	γCC (25) + βHCC (28)
63			1295	1245	1	0	27	2	γCC (46)
62	1221		1275	1225	70	15	66	5	γCC (34) + βHCC (27)
61		1212	1263	1213	32	7	2	0	γNC (24) + βHNC (23) + βHCC (14)
60			1239	1191	83	17	56	4	γNC (25) + βHCC (14)
59		1167	1198	1151	135	28	26	2	γNC (19) + βHCC (26)
58			1171	1125	94	19	18	1	γCC (13)
57			1163	1118	21	4	278	20	γNC (20) + γCC (10)
56			1137	1093	164	34	8	1	γFC (19) + βHCC (14)
55			1133	1089	77	16	20	1	γCC (28) + βHCC (12) + βCCC (12)
54			1126	1082	220	46	2	0	γFC (78) + ωFCFC (12)
53	1055	1052	1109	1065	40	8	35	3	γFC (12) + βHCC (35)
52			1081	1039	14	3	13	1	γFC (35) + γClC (11)
51	999		1044	1003	60	13	24	2	γCC (48) + βHCC (314)
50			1003	964	3	1	36	3	γCC (11) + βCCC (48)
49			978	940	1	0	7	1	βCCN (20)
48			960	922	0	0	0	0	τHCCC (77) + τCCCC (11)
47	899	887	920	884	26	5	6	0	τHCCC (44) + τHCCN (28) + τCCCC (13)
46			914	878	20	4	2	0	τHCCC (24)
45			906	871	18	4	4	0	τHCCC (46)
44	866		892	857	11	2	28	2	τHCCC (70)
43			849	816	19	4	8	1	βCCC (39)
42			827	795	34	7	1	0	τHCCC (78)
41			803	772	4	1	27	2	τHCCC (34) + τHCCN (55)
40	749	748	784	753	5	1	1	0	τCCCN (14) + τCCCC (12) + ωONCC (37) + ωNCCC (15)
39	733		745	716	12	2	4	0	βCCC (19)
38			734	705	4	1	2	0	ωCCCC (10)
37			731	703	1	0	0	0	τCCCC (22) + ωCCCC (11)
36		684	707	680	34	7	29	2	βCCC (15)
35	666		691	664	5	1	2	0	βCCC (31) + βCNC (16)
34			675	649	21	4	7	0	βCCC (17)
33			658	632	16	3	4	0	ωFCFC (12) + ωNCCC (22)
32			627	603	1	0	4	0	βOCN (18)

31			613	589	13	3	33	2	τCCNC (13)
30	566	571	582	560	7	1	3	0	βFCF (12) + ωFCFC (16)
29			557	535	2	0	5	0	βCNC (10)
28		522	535	514	6	1	9	1	τHNCC (17)
27			530	509	26	5	6	0	βNCC (13) + τHNCC (30)
26			516	496	45	9	18	1	βFCF (27) + τCCCC (24)
25			474	456	33	7	10	1	γClC (14) + βFCF (11)
24			464	446	4	1	11	1	τHNCC (32) + ωNCCC (11)
23			440	423	12	2	1	0	βFCF (10) + τCCCC (21)
22			433	416	11	2	2	0	τCCCC (17)
21			411	395	2	0	11	1	βBrCC (14) + ωClCCC (13)
20			374	360	8	2	11	1	βFCF (22) + τCCCC (11) + ωFCFC (17)
19		341	356	342	4	1	4	0	ωBrCCC (36) + ωNCCC (19)
18			340	326	5	1	7	0	γCC (13) + βFCF (18) + ωFCFC (13)
17			322	309	3	1	9	1	τCCCC (11) + ωClCCC (12)
16			305	293	1	0	2	0	γBrC (51)
15			295	284	0	0	3	0	βClCC (29)
14		269	272	261	1	0	9	1	βOCN (13) + βNCC (12) + βCCN (12) + βBrCC (15)
13			249	240	0	0	11	1	βHCC (18)
12			217	208	2	0	2	0	βCNC (10) + βCCC (21) + βBrCC (12)
11		178	166	160	1	0	2	0	βCCC (27) + βClCC (15)
10		159	160	154	0	0	4	0	τCCCC (11) + τCCCC (45) + ωBrCCC (27)
9			144	139	0	0	0	0	βBrCC (10) + ωCCCC (21)
8		127	124	119	1	0	29	2	τCCCC (33)
7		114	115	111	1	0	3	0	τCCCC (48)
6			90	86	1	0	4	0	βNCC (13) + τCCCC (13) + τCNCC (14) + τCCNC (11)
5		75	71	68	1	0	2	0	τFCCC (80)
4			50	48	0	0	1	0	τCCCC (10)
3			31	30	1	0	4	0	βNCC (11) + τCCCN (42) + τCCNC (18)
2			24	23	0	0	2	0	βCNC (35) + βCCN (11) + ωNCCC (20)
1			12	11	1	0	7	1	τCNCC (75)

[a]Scaling factor: 0.961 for B3LYP/6-311++G(d,p). [b]Relative IR absorption normality intensities with highest peak absorption equal to 100. [c]Relative Raman intensities normalized to 100. [d]γ - stretching, β - bending, τ - torsion, ω - put-of-plane bending.

Molecular electrostatic potential (MEP): In the MEP map, of the optimized structure of the title compound in gas phase is shown in Fig. 3 and the colour-coded zone extends from -7.028e^{-2} (red) to 7.028e^{-2} (blue). Red and yellow on MEP surfaces show the electron-rich regions that promote electrophilic attack, whereas the green region suggests the neutral sites and blue indicates electron-accepting sites that support nucleophilic attack [26,27].

NBO: The steady energy between donor-acceptor levels were also calculated and then second-order perturbation theory was typically applied. Single-pair calculations were performed to analyze stability, bonding descriptions, intramolecular and intermolecular linkages, electron donors within a system and unoccupied orbitals of electron acceptors in other systems. As the orbitals are computationally chosen to maximize the proportion of charge distribution, NBO analysis offers the most accurate description of the potential Lewis structures [28]. Table-3 displays the calculated stabilized energies between donor-acceptor pairs in the central molecule. The largest energy equilibrium (268.09 kcal/mol) was found between π*(C14-C15) and π*(C2-C5), whereas π*(C16-C17) and π*(C12-C13) interacted to produce a state of equilibrium energy of 226.43 kcal/mol, was the next-highest. Next, the stabilization energy is 136.44 kcal/mol for LP2-O10 to σ*(N1-C2), respectively.

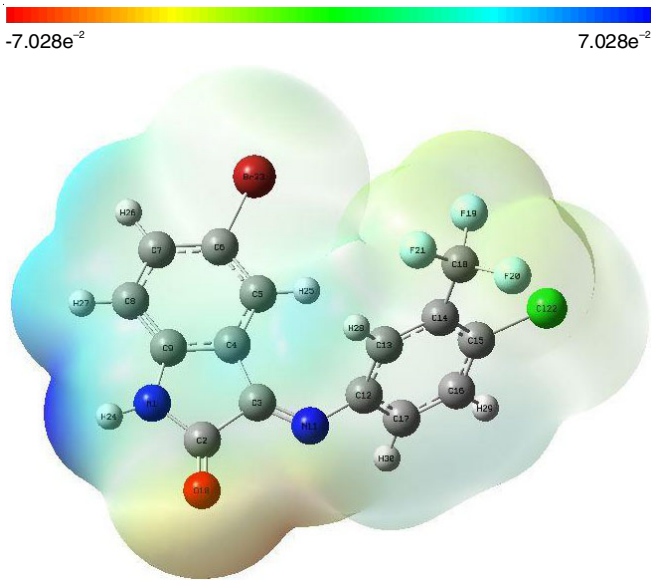

Fig. 3. MEP surface image of 5BTPIO molecule

TABLE-3
SECOND ORDER FOCK MATRIX (NBO) OF 5BTPIO MOLECULE

Type	Donor (i)	ED/e	Type	Acceptor (j)	ED/e	$E^{(2)}$ (kJ/mol)[a]	E(j)-E(i) (a.u.)[b]	F(i,j) (a.u.)[c]
σ	C16-C17	0.0148	σ*	C16-H29	0.01278	5.12	1.15	0.069
σ	C16-C17	0.0148	π*	C3-N11	0.01572	4.39	0.29	0.034
σ	C7-C8	0.01521	σ*	C13-C14	0.02014	4.86	1.29	0.071
σ	C13-C14	0.02014	σ*	N1-C9	0.0256	5.71	1.13	0.072
σ	C4-C5	0.02556	σ*	N11-C12	0.02805	5.68	1.07	0.070
π*	C12-C13	1.62886	σ*	C15-Cl22	0.02902	5.38	0.86	0.061
π*	C12-C13	1.62886	σ*	C15-Cl22	0.02902	4.87	0.87	0.058
π*	C8-C9	1.64728	σ*	C6-Br23	0.03234	5.03	0.80	0.057
π*	C8-C9	1.64728	σ*	C6-Br23	0.03234	5.00	0.81	0.057
π*	C4-C5	1.6584	σ*	C14-C18	0.05712	5.92	0.78	0.061
π*	C4-C5	1.6584	σ*	C14-C18	0.05712	5.86	0.77	0.060
π*	C4-C5	1.6584	σ*	C14-C18	0.05712	5.81	0.77	0.060
π*	C16-C17	1.66656	π*	C12-C13	1.62886	226.43	0.02	0.084
π*	C16-C17	1.66656	π*	C12-C13	1.62886	20.54	0.28	0.068
π*	C6-C7	1.67058	π*	C12-C13	1.62886	18.59	0.30	0.068
π*	C6-C7	1.67058	π*	C12-C13	1.62886	13.51	0.36	0.066
π*	C6-C7	1.67058	π*	C8-C9	1.64728	38.93	0.29	0.096
LP(1)	N1	1.67369	π*	C8-C9	1.64728	22.81	0.28	0.072
LP(1)	N1	1.67369	π*	C8-C9	1.64728	15.15	0.29	0.060
π*	C14-C15	1.68196	π*	C4-C5	1.65840	268.09	0.01	0.082
π*	C14-C15	1.68196	π*	C4-C5	1.65840	22.73	0.29	0.074
π*	C14-C15	1.68196	π*	C14-C15	1.65840	22.71	0.27	0.071
π*	C14-C15	1.68196	π*	C14-C15	1.65840	20.87	0.26	0.068
LP(2)	O10	1.8442	π*	C4-C5	1.65840	16.43	0.29	0.062
LP(1)	N11	1.8442	π*	C16-C17	1.66656	136.44	0.02	0.081
LP(1)	N11	1.8442	π*	C16-C17	1.66656	18.57	0.29	0.067
LP(1)	N11	1.8442	π*	C16-C17	1.66656	18.39	0.31	0.067
LP(2)	F19	1.93683	π*	C6-C7	1.67058	24.14	0.28	0.074
LP(2)	F21	1.94125	π*	C6-C7	1.67058	17.04	0.27	0.062
LP(2)	F20	1.95189	σ*	C14-C15	1.68196	5.41	0.86	0.061
σ	C13-C14	1.96391	π*	C3-N11	1.90162	17.77	0.29	0.067
σ	C14-C15	1.96391	σ*	C2-C3	1.96487	23.09	0.61	0.107
σ	C2-C3	1.96487	σ*	C2-C3	1.96487	5.58	0.69	0.056
σ	C7-C8	1.96694	σ*	C3-C4	1.97218	14.96	0.79	0.100
LP(2)	Cl22	1.96748	σ*	C14-C15	1.97467	5.6	1.26	0.075
σ	C12-C17	1.96875	π*	C2-O10	1.97705	50.58	0.29	0.111
σ	C12-C17	1.96875	σ*	N1-C2	1.98855	28.15	0.68	0.125
ν*	C12-C13	1.96875	σ*	C18-F20	1.99404	9.11	0.95	0.085
σ	C17-H30	1.97829	σ*	C18-F21	1.99542	35.89	4.36	0.358
σ	C17-H30	1.97829	σ*	C18-F21	1.99542	34.68	4.17	0.345
LP(2)	O10	1.97963	σ*	C18-F21	1.99542	6.53	4.37	0.153

NLO: This investigation assessed the NLO behaviour of the referenced material. Table-4 displays the calculated values of the titled compound. The total dipole moment is 2.116 Debye. The polarizability and hyperpolarizability were measured at 7.992×10^{-23} e.s.u. and 1.037×10^{-29} e.s.u., respectively. The values particularly hyperpolarizability highlight the strong NLO response of 5BTPIO, making it a capable material for future optical applications. Thus, its potential impact on the biology systems further emphasizes its versatility and broader scientific importance.

Electron localization function (ELF) and localized orbital locator (LOL): The electron pair density was calculated using a Multiwfn software [29]. As seen in Fig. 4 the colour coding designates a location for 5BTPIO molecule with strong ELF and LOL values. The exact centroid of electron pair density and the LOL model is the constrained electron cloud [30]. The ELF colour code, which ranges from blue to red, represents molecular characteristics that vary from 0 to 1 for the Bohr electron mass range of -11.94 to 11.94. Localized bonds and non-bonded electrons are indicated by a value < 0.5, whereas bonded electrons are indicated by a value > 0.5. On the ELF map, low-density electrons are shown in blue, while high-density, delocalized electrons are depicted in red around the high hydrogen atom (H_{26}). When the interaction changes from weaker to stronger neighboring reactions and *vice versa*, the density gradient characteristic decreases, which explains the non-shared interaction.

NMR analysis: A new method for identifying and predicting the molecular structure of large macromolecules combines

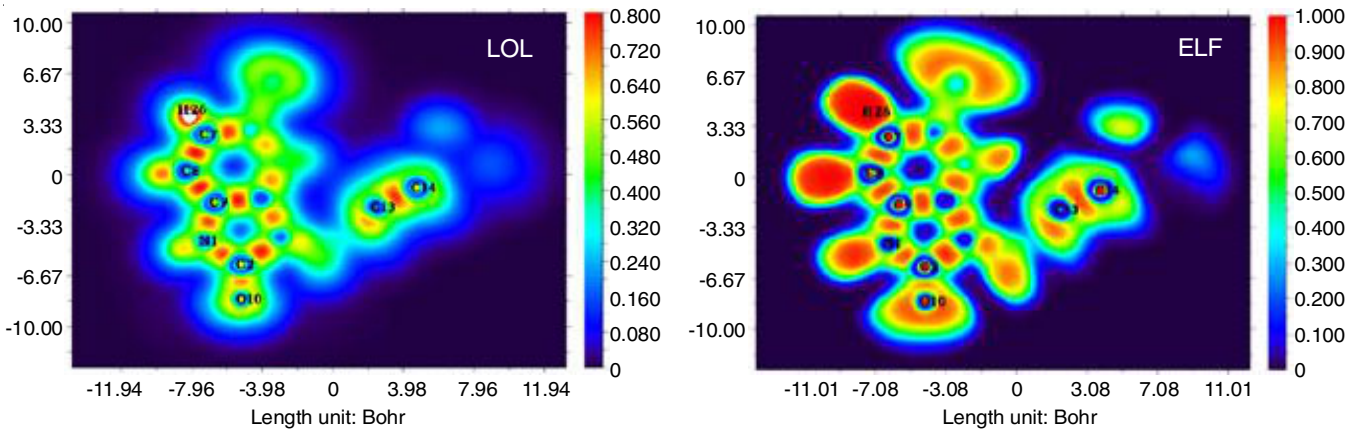

Fig. 4. ELF and LOL of 5BTPIO molecule

TABLE-4
NLO PARAMETERS OF 5BTPIO IN GAS PHASE

Parameters	Values	Parameters	Values
μx	-1.987	Δα (e.s.u)	7.992×10^{-23}
μy	0.466	βxxx	-1316.258
μz	-0.557	βxxy	-275.294
μ(D)	2.116	βxyy	164.849
αxx	302.575	βyyy	35.75
αxy	20.767	βzxx	110.171
αyy	253.911	βxyz	56.313
αxz	-31.651	βzyy	-66.863
αyz	2.033	βxzz	-31.981
αzz	158.108	βyzz	39.695
α (a.u)	238.198	βzzz	-89.24
α (e.s.u)	3.530×10^{-23}	βtot (a.u)	1201.024
Δα (a.u)	539.317	βtot (e.s.u)	1.0376×10^{-29}

TABLE-5
^{1}H AND ^{13}C NMR CHEMICAL SHIFTS VALUES OF 5BTPIO

Atoms	Chemical shifts (ppm)	
	Calculated	Experimental
29-H	7.58	7.5
26-H	7.285	7.255
28-H	7.185	7.1
30-H	7.055	7
25-H	6.831	6.83
24-H	6.406	6.42
2-C	164.9	163.84
15-C	143.87	143.02
18-C	132.44	132.2
17-C	125.99	125.2
13-C	118.99	118.52
8-C	113.68	113.38

computer modeling and NMR spectroscopic method. The B3LYP/6-311G++(d,p) basis level GIAO technique has been utilized to extract the optimized structure (^{13}C and ^{1}H) of title compound. Table-5 presents the findings obtained through theoretical and experimental methods. The chemical shifts of the carbon atoms at locations C8 and C17 are 113.38 and 125.2 ppm, respectively. The 2C atom has a chemical shift of 164.9 ppm and 163.84 ppm, respectively, both in theory and in practice. The indolin ring's proton, H24, is observable at a lower chemical shift of 6.420 ppm and 6.406 ppm. Both experimentally and theoretically, values can be computed. Signals observed at 7.58, 7.285, 7.185, 7.055 and 6.831 ppm theoretically imply the presence of aromatic hydrogen atoms (H29, H26, H28, H25 and H30) in the phenyl ring. The values of the experiment were 7.5, 7.25, 7.1, 7.0 and 6.83 ppm. Almost all the signals correspond effectively with the experimental results, except in cases when experimental and theoretical results varied.

Fukui function: The Fukui function is associated with the local softness and both differ at the specific points between electrophilic and nucleophilic attacks [31]. The results for dual-characterizing properties, which local softness, Fukui function and Mulliken charges, are presented in Table-6. Oxygen is identified as the ideal target for an electrophilic attack. Considering the electronegativity of nitrogen atom, the carbon atom becomes the electron-deficient and more susceptible to nucleophilic. Electrophilic attacks are found around the atoms C2, C3, C5, C7, O10, N11, C14, C15, H24, H25, H26 and H27. Nucleophilic attacks are identified at N1, C4, C6, C8, C9, C12, C13, C16, C17, C18, F19, F20, F21, Cl22, Br23, H28, H29 and H30.

Interaction region indicator (IRI) and reduced density gradient (RDG) analysis: The interaction region indicator (IRI) is especially useful for studying various molecular structures and chemical reactions since it can identify the weaker contact zones within molecules. The ability of IRI to identify the chemical interactions inside biomolecules depends on electron density [32]. The blue isosurfaces point to strong, electron-dense connections, green isosurfaces mark weak interactions and red isosurfaces indicate steric clash or repulsion (Fig. 5). Effective interactions, specifically for C–C connections, are identified when π-electrons converge within the aromatic ring. To visualize in a better manner, these non-covalent interactions (NCI), researchers use a technique called reduced density gradient (RDG) analysis [33]. This demonstrates that the electron dispersion of the particle is no longer impartial. The type of interactions within a molecule can then be discerned by examining the direction of the second derivative of electron density or Hessian parameter $(\lambda 2)\rho$ [34]. To visualize the weak connections in real space, we have created colour-banded reduced

TABLE-6
FUKUI FUNCTION OF 5BTPIO MOLECULE

Atom	Mulliken atomic charges			Fukui functions			Δf(r)
	0,1 (N)	N+1 (-1,2)	N-1 (1,2)	f_r^+	f_r^-	f_r^0	
1N	-0.21386	-0.2261	-0.17185	-0.012	-0.042	-0.027	0.03
2C	0.125379	0.12698	0.074808	0.002	0.051	0.026	-0.049
3C	-0.5718	-0.62396	-0.52823	-0.052	-0.044	-0.048	-0.009
4C	1.373262	1.389195	1.38991	0.016	-0.017	0	0.033
5C	-0.91821	-0.91081	-0.96622	0.007	0.048	0.028	-0.041
6C	0.053008	-0.12349	0.247015	-0.176	-0.194	-0.185	0.018
7C	0.052761	0.030497	0.037431	-0.022	0.015	-0.003	-0.038
8C	-0.56842	-0.55711	-0.56703	0.011	-0.001	0.005	0.013
9C	-0.08112	-0.06369	-0.07258	0.017	-0.009	0.004	0.026
10O	-0.29677	-0.41094	-0.2052	-0.114	-0.092	-0.103	-0.023
11N	0.284785	0.165804	0.353804	-0.119	-0.069	-0.094	-0.05
12C	-1.0903	-1.08087	-1.09608	0.009	0.006	0.008	0.004
13C	-0.31083	-0.27017	-0.28943	0.041	-0.021	0.01	0.062
14C	-0.70186	-0.74252	-0.68241	-0.041	-0.019	-0.03	-0.021
15C	0.719596	0.728596	0.698797	0.009	0.021	0.015	-0.012
16C	-0.57016	-0.59381	-0.54675	-0.024	-0.023	-0.024	0
17C	0.543565	0.491513	0.56734	-0.052	-0.024	-0.038	-0.028
18C	0.45781	0.457403	0.461159	0	-0.003	-0.002	0.003
19F	-0.03844	-0.0529	-0.02205	-0.014	-0.016	-0.015	0.002
20F	-0.04127	-0.06199	-0.01799	-0.021	-0.023	-0.022	0.003
21F	-0.1382	-0.14791	-0.12263	-0.01	-0.016	-0.013	0.006
22Cl	0.525585	0.435898	0.673066	-0.09	-0.147	-0.119	0.058
23Br	-0.14452	-0.24515	-0.00203	-0.101	-0.142	-0.122	0.042
24H	0.345175	0.298985	0.385724	-0.046	-0.041	-0.043	-0.006
25H	0.165867	0.132235	0.168685	-0.034	-0.003	-0.018	-0.031
26H	0.234575	0.183728	0.277032	-0.051	-0.042	-0.047	-0.008
27H	0.161428	0.108982	0.208364	-0.052	-0.047	-0.05	-0.006
28H	0.212207	0.200125	0.238154	-0.012	-0.026	-0.019	0.014
29H	0.218499	0.18081	0.260568	-0.038	-0.042	-0.04	0.004
30H	0.212246	0.180641	0.248629	-0.032	-0.036	-0.034	0.005

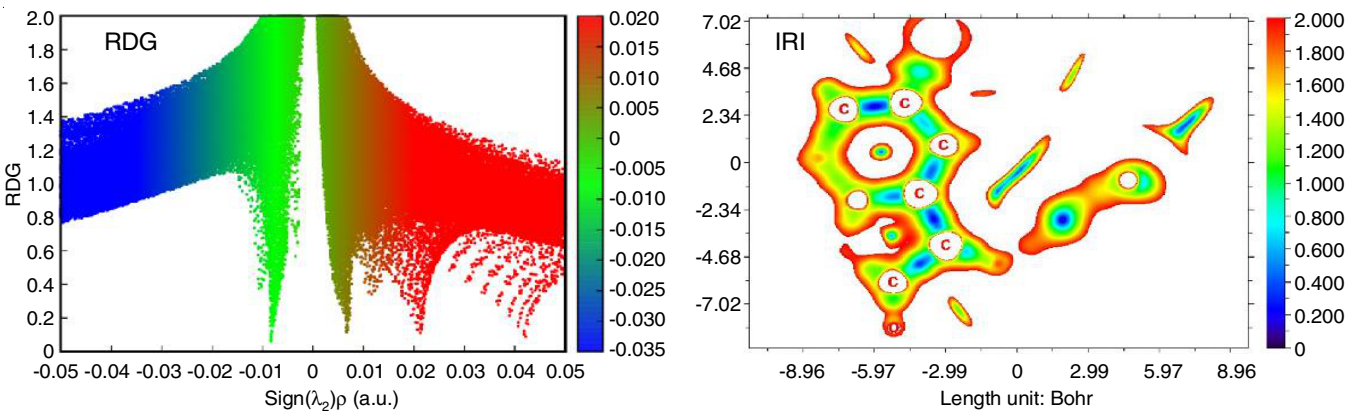

Fig. 5. Reduced density gradient (RDG) and interaction region indicator (IRI) of 5BTPIO molecule

density gradient (RDG) mappings. These RDG plots, generated for the gas phase. Different interactions are recognized by their respective colour codes: blue for hydrogen bonding, green for van der Waals (VdW) attraction and red for steric repulsion. Strong repulsions, visible as an elliptical red layer in the core rings, exert considerable steric influence and are associated with C–C stacked interactions involving amino groups and the rings. Separately, a green-red patchy flaky zone between 0.00 and 0.01 au suggests a weak VdW attractive interaction due to low electron density. The absence of blue surges between 0.01 and 0.05 a.u. in the RDG analysis confirms that diamino groups and rings do not form significant noncovalent interactions (NCI) or hydrogen bonds. The image also features an aqua ringed band, spread across it, which represents an H-bond within the structure of molecule. This observation demonstrates strong agreement between the IRI and RDG data.

Charge transfer: The study of holes and electrons provides a considerable insight into the excitation behaviour of electrons [35]. Most absorption spectrum transitions occur among the lowest energy state and three consecutive states; however, studies

on electron-hole systems remains limited to these three states [36]. The Multiwfn [37] was employed to calculate the charge transfer dispersal, which illustrates the electron-hole transition, or the charge movement between the electron and the hole (Fig. 6). Table-7 are comparable, with blue representing holes and green representing electrons. The first excited state shows the holes around carbon and oxygen atoms, whereas electrons encircle the ring systems in second and third states. The increase in Δr under identical conditions highlights enhanced charge transfer during the third excitation phase.

TABLE-7
EXCITATION ENERGY (E), D INDEX, Δr INDEX, t INDEX FOR DIFFERENT EXCITED STATES FOR 5BTPIO IN GAS PHASE

Parameters	Excited state		
	First	Second	Third
Excitation energy E (eV)	2.476	2.678	3.675
Charge transfer length D index (Å)	2.311	2.01	1.89
Δr index (Å)	2.7	1.986	1.678
t index (Å)	0.297	0.148	0.523

Ramachandran plot: Ramachandran plots were used to assess the binding affinity. The anticancer properties of material were predicted using the online tool PASS [38]. Their validity was subsequently verified through the superimposition of their amino acid sequences onto Ramachandran plots [39]. Fig. 7 illustrates a Ramachandran plot for three docked anticancer antigens, indicating that 90% of the amino acids reside within the acceptable (green) zone. This indicates that a minimal number of amino acids reside in restricted areas, illustrating the stable conformation of protein for binding. All the protein consistently display a high concentration of residues within the red permissible domains, with only a minimal presence in the black restricted domains. Moreover, proteins 6EGR, 6ETJ and 6VHG are conformationally appropriate for docking.

Drug likeness: Drug development relies heavily on drug similarity analysis. Drug-likeness computations were performed using the Swiss ADME portal [40]. According to this tool, HBD and HBA scores shouldn't be higher than 10 and 5, respectively, however, 5BTPIO has HBD values of 0 and HBA values of 3. TPSA has a maximum score of 41.46 and the molecule's MR characteristic is 88.18 cm/s, which aligned with the typical range of 40 to 130 (Table-8).

Lipinski's rule of five [41] plays a vital role in identifying the suitability of drugs. This rule helps to predict whether a lead molecule will be effective as a therapeutic agent once it's absorbed into the body. A key physico-chemical characteristic influencing drug similarity is the lipophilicity, which demonstrates that molecules have the required traits for a substance to act as a prescription drug. The results indicate that 5BTPIO possesses the expected pharmacokinetic radar and boiled-egg plot characteristics [42]. As shown in Fig. 8, 5BTPIO aligns with the bioavailability radar parameters. Thus, the title molecule exhibits the characteristics required for drug activity and the results confirmed its significant bioactivity.

TABLE-8
DRUG-LIKENESS VALUES OF 5BTPIO MOLECULE

Descriptor	Value	Optimum range (Yes/No)
Hydrogen bond donors (HBD)	1	Yes
Hydrogen bond acceptors (HBA)	5	Yes
Log P	2.54	Yes
Number of atoms	23	Yes
Number of rotatable bonds	2	Yes
Molecular weight	403.6	Yes
Molar refractivity	88.8	Yes
TPSA	41.46	
Fraction CSP3	0.07	
Lipophilicity details		
iLOGP	2.78	
XLOGP	4.76	
WLOGP	5.77	
MLOGP	3.95	
Silicos-IT	5.58	
Consensus Logp	4.57	

Molecular docking: The PatchDock online website is a crucial tool for pharmaceutical development, particularly in the ligand-protein interaction studies. The interaction among a ligand and a protein aims to predict the ligand's preferred binding orientation(s) with a specific 3D structure of the protein [43]. The target protein structures selected for the anticancer study of the 5BTPIO were acquired in RCSB PDB format [44]. Fig. 9 illustrates the interactions of 5BTPIO ligand with each of these target proteins. The binding energies for target proteins 3G74, 4Z8Z and 7PGL were determined to be -6.08, -5.60 and -6.72 kcal/mol. Of these, 7PGL displayed the strongest binding affinity. Conversely, 4Z8Z recorded the lowest binding energy and intermolecular energy in its protein-ligand interaction. The interaction of 5BTPIO with all target proteins affirms

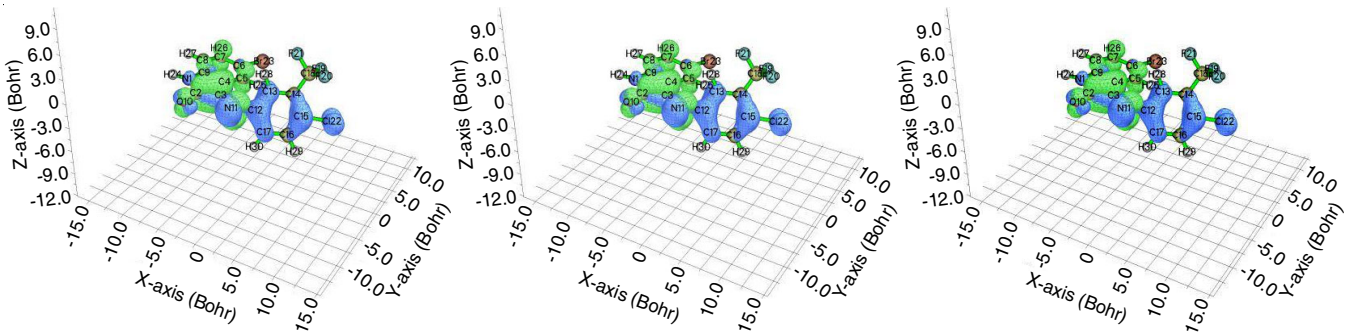

Fig. 6. Charge transfer of 5BTPIO molecule

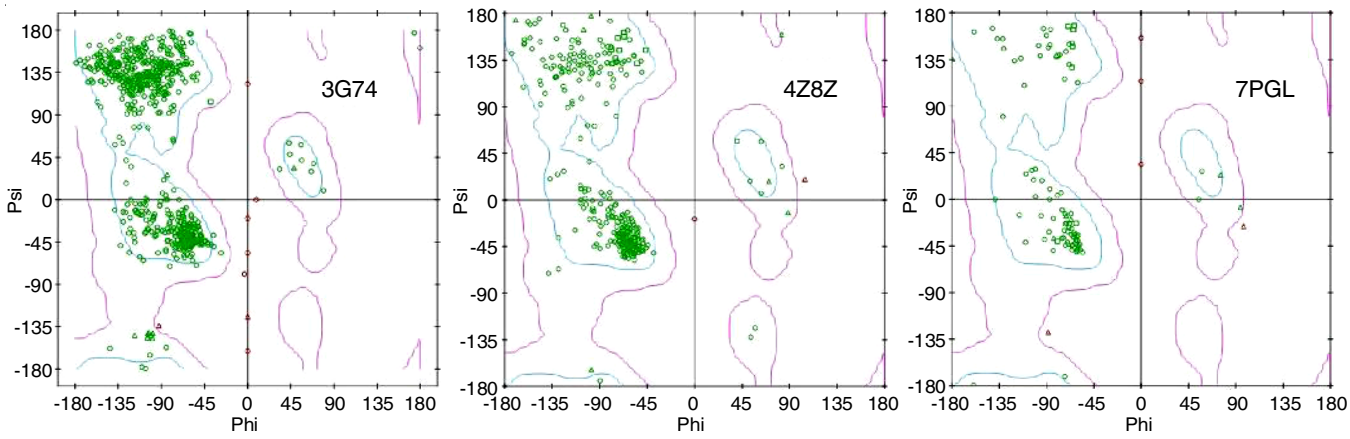

Fig. 7. Ramachandran plot of proteins

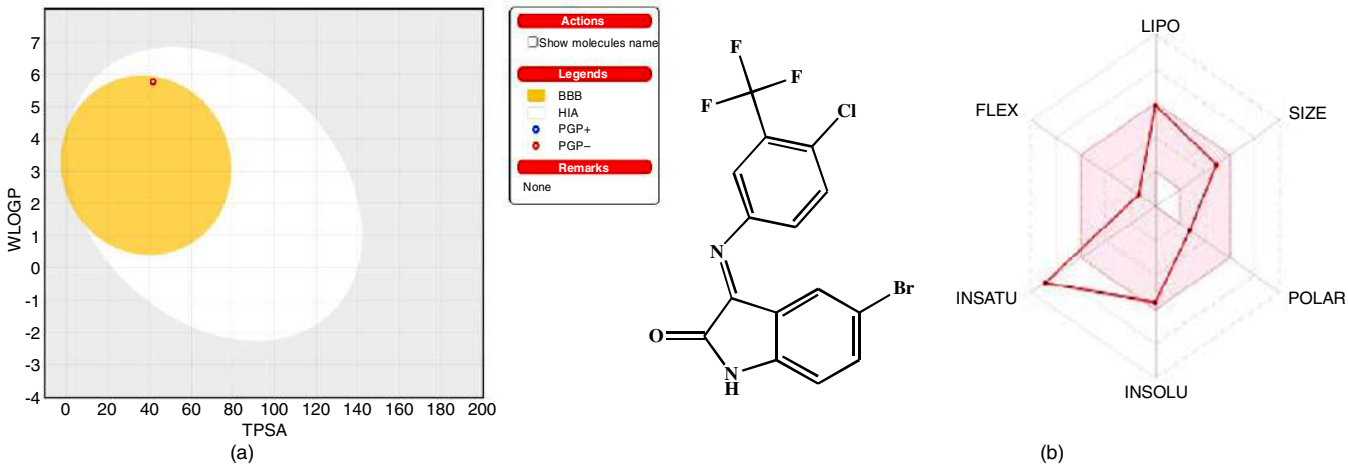

Fig. 8. Drug-likeness properties of 5BTPIO molecule

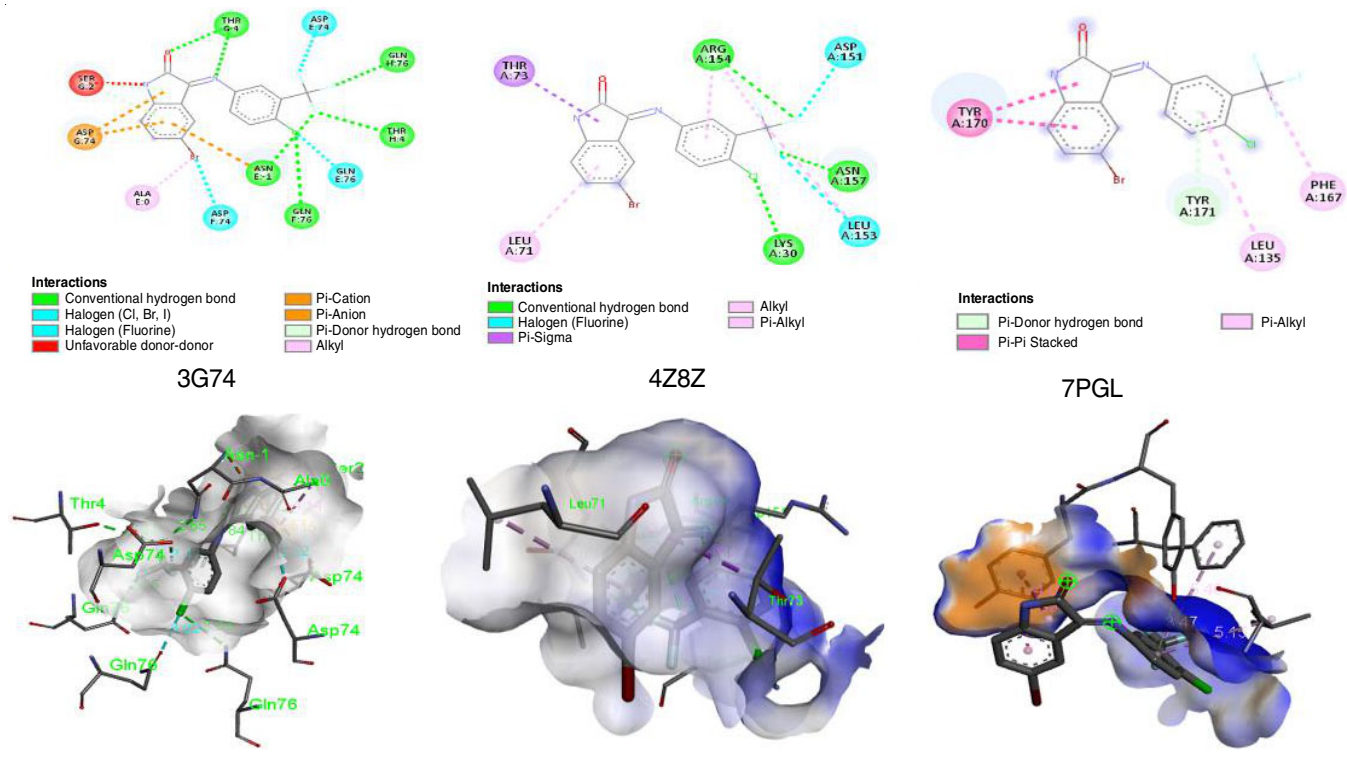

Fig. 9. 2D and 3D protein-ligand interactions of 5BTPIO with selected proteins

its bioactivity and the good interactions are observed between the residues of both proteins, with bond distances as highlighted in Table-9. Atomic contact energy was employed to identify more stable complexes, which ultimately indicates that 5BTPIO and the proteins effectively collaborate pharmacologically.

TABLE-9
INTERACTION ENERGY ANALYSIS OF 5BTPIO WITH TARGETED PROTEIN USING PATCH DOCK

Target protein	ACE (-kcal/mol)	Inhibition constant	Interaction of 5BTPIO residue	Bond distance (Å)
3G74	-6.08	78.31	ASn E:-1	2.65
			GLN E:76	2.15
			GLN H:76	3.02
			THR H:4	3.8
			GLN F:76	3.24
			ASP E:74	3.12
			THR G:4	2.31
			SER G:2	3.13
			ASP G:74	3.43
			ALAE :0	1.14
			ASP G:74	3.12
4Z8Z	-5.6	54.88	LEU A:71	5.27
			LYS A:30	3.46
			LEU A:153	3.5
			ASN A:157	2.61
			ASP A:151	3.45
			ARG A:154	4.62
			THR A:73	3.84
7PGL	-6.72	62.98	LEU A:135	5.15
			PHE A:167	4
			TYR A:171	4.09
			TYR A:170	3.47

Anticancer activity: The *in vitro* anticancer activity of the synthesized compound was characterized by the National Cancer Institute (NCI) against sixty human cancer cell lines under the developing therapeutics program (DTP). At a concentration of 10^{-5} M, 5BTPIO was screened against nine panels of cancer cell lines at one dose. DTP generated an NSC (D-833719/1) code that could be used to retrieve the inhibitory effects of compound from the NCI database. According to the one-dose screening report of DTP, the growth inhibition (GI) of cancer cells by the compound was calculated using the % GI = 100 – growth % formula [45]. It was observed that 30 human cancer cell lines showed inhibition and the remaining cancer cell lines were not inhibited by 5BTPIO (Fig. 10). Synthesized hybrid 5BTPIO is shown to inhibit the CCRF-CEM cancer cell line in the leukemia panel, exhibiting 12.88% GI. According to the non-small cell lung cancer panel, the 5BTPIO also restricted the growth of EKVX, NCI-H23, NCI-H322M and NCI-H522 cancer cell lines, which displayed 4.27, 0.11, 8.83 and 3.83% GI, respectively. Four cancer cell lines (HCT-15, HT29, KM12 and SW-620) were inhibited under the colon cancer subpanel and their respective GI % was 26.18, 3.46, 5.36 and 13.24%, respectively.

After being inhibited, five cancer cell lines from the central nervous system (SF-268, SF-295, SF-539, SNB-19 and U251) were found to have 2.27, 6.95, 8.53, 5.57 and 15.69% GI, respectively. In comparison, four cancer cell lines (LOX IMVI, MALME-3M, M14, MDA-MB-435 and UACC-62) within the melanoma sub-panel were inhibited and exhibited % of GI of 10.35, 3.43, 2.24, 41.82 and 33.73. Furthermore, the 5BTPIO restricted the growth of three ovarian cancer cell lines, IGROV1, OVCAR-3 and OVCAR-8, which had 4.44, 21.75 and 0.91% GI, respectively. The next renal cancer panel revealed 15.29, 14.66, 12.47 and 26.61% GI, respectively, throughout a maximum of four sub-panels (ACHN, CAKI-1, SN12C and UO-31). Only the PC-3 cancer cell line was found to be 3.21% resistant to growth inhibition. Three cancer cell lines of breast cancer (MCF7, MDA-MB-231/ATCC and T-47D) displayed 48.81, 17.01 and 9.43% GI, respectively. Moreover, the suggested synthesized 5BTPIO exhibited the highest activity (48.81% GI) against the breast cancer cell line MCF7. Thus, based on the above said facts, in future, this compound may be derivatized to develop a medication that is more effective against breast cancer.

Conclusion

A comprehensive study of synthesized (*E*)-5-bromo-3-((4-chloro-(trifluoromethyl)phenyl)imino)indolin-2-one (5BTPIO) consisted the experimental and computed spectral data has been characterized. DFT computations at B3LYP/6-311++G(d,p) level of theory optimized the gas-phase geometry, showing a C6–Br23 bond length of 1.915 Å and a C4–C3–N11 bond angle of 134.5º. The molecule was characterized with FT-IR, ^{1}H, ^{13}C NMR and FT-Raman spectroscopy. Vibrational spectra were compared with FT-IR and FTR data, correlating key wavenumbers. Preliminary biological tests also explored its potential pharmacological activity. Prominent interactions include π*(C14–C15) to π*(C2–C15) with the highest stabilization energy of 268.09 kcal/mol. Fukui Function identified stable electrophilic and nucleophilic assaults. Pharmacological analysis and ADMET profiling of 5BTPIO revealed that it adheres to various medicinal chemistry parameters, falling within acceptable ranges. The molecule successfully docked against cancer targets, demonstrating potent anticancer activity. The study states that the suggested synthesized compound exhibited the highest activity (48.81% GI) against the breast cancer cell line MCF7. In the future, this molecule may be enhanced to develop a more effective medicine for breast cancer.

CONFLICT OF INTEREST

The authors declare that there is no conflict of interests regarding the publication of this article.

REFERENCES

1. K.N. Venugopala, M. Kandeel, M. Pillay, P.K. Deb, H.H. Abdallah, M.F. Mahomoodally and D. Chopra, *Antibiotics*, **9**, 559 (2020); https://doi.org/10.3390/antibiotics9090559
2. M. Asif, F. Aqil, F.A. Alasmary, A. almalki, A.R. Khan and M. Nasibullah, *Med. Chem. Res.*, **32**, 1001 (2023); https://doi.org/10.1007/s00044-023-03053-7
3. S. Khalid, S.H. Sumrra and Z.H. Chohan, *Sains Malays.*, **49**, 1891 (2020); https://doi.org/10.17576/jsm-2020-4908-11
4. M. Asif, T. Azaz, B. Tiwari and M. Nasibullah, *Tetrahedron*, **134**, 133308 (2023); https://doi.org/10.1016/j.tet.2023.133308

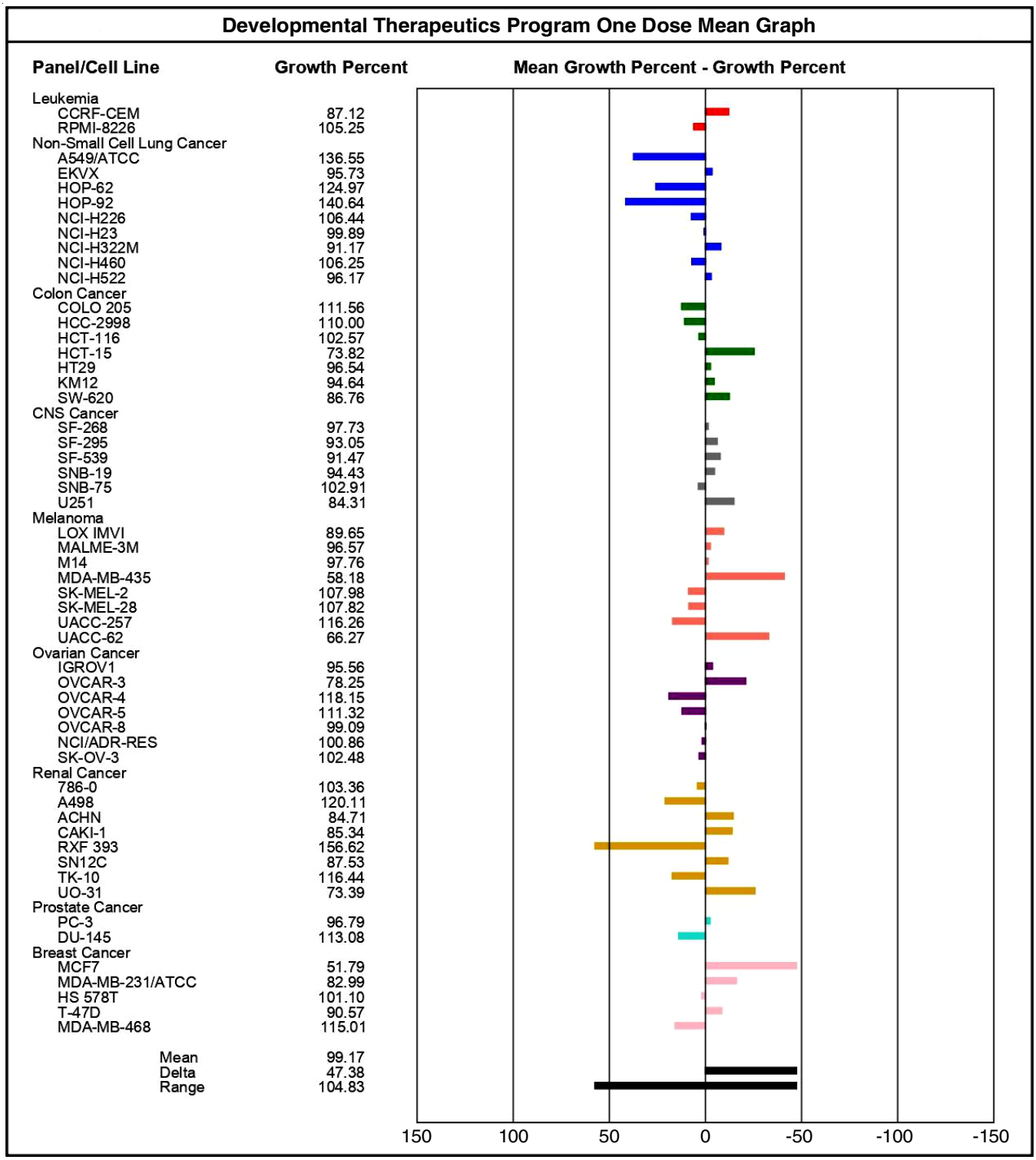

Fig. 10. One-dose mean graph for showing % GI against 60 human cancer cell lines

5. M. Asif, S.S. Alvi, T. Azaz, A.R. Khan, B. Tiwari, B.B. Hafeez and M. Nasibullah, *Int. J. Mol. Sci.*, **24**, 7336 (2023); https://doi.org/10.3390/ijms24087336
6. V.S.J. Reeda, V.B. Jothy, M. Asif, M. Nasibullah, S. Kadaikunnan, G. Abbas and S. Muthu, *J. Mol. Struct.*, **1294**, 136310 (2023); https://doi.org/10.1016/j.molstruc.2023.136310
7. M. Amirmostofian, J.P. Jaktaji, Z. Soleimani, K. Tabib, F. Tanbakosazan, M. Omrani and F. Kobarfard, *Iran. J. Pharm. Res.*, **12**, 255 (2013).
8. S. Nussbaumer, P. Bonnabry, J.-L. Veuthey and S. Fleury-Souverain, *Talanta*, **85**, 2265 (2011); https://doi.org/10.1016/j.talanta.2011.08.034
9. P. Dhokne, A.P. Sakla and N. Shankaraiah, *Eur. J. Med. Chem.*, **216**, 113334 (2021); https://doi.org/10.1016/j.ejmech.2021.113334
10. P. Dey, A. Kundu, S.H. Han, K.-S. Kim, J.H. Park, S. Yoon, I.S. Kim and H.S. Kim, *Biomolecules*, **10**, 1260 (2020); https://doi.org/10.3390/biom10091260

11. M.J. Frisch, G.W. Trucks, H.B. Schlegel, G.E. Scuseria, M.A. Robb, J.R. Cheeseman, G. Scalmani, V. Barone, B. Mennucci, G.A. Petersson, H. Nakatsuji, M. Caricato, X. Li, H.P. Hratchian, A.F. Izmaylov, J. Bloino, G. Zheng, J.L. Sonnenberg, M. Hada, M. Ehara, K. Toyota, R. Fukuda, J. Hasegawa, M. Ishida, T. Nakajima, Y. Honda, O. Kitao, H. Nakai, T. Vreven, J.A. Montgomery, J.E. Peralta Jr., F. Ogliaro, M. Bearpark, J.J. Heyd, E. Brothers, K.N. Kudin, V.N. Staroverov, T. Keith, R. Kobayashi, J. Normand, K. Raghavachari, A. Rendell, J.C. Burant, S.S. Iyengar, J. Tomasi, M. Cossi, N. Rega, J.M. Millam, M. Klene, J.E. Knox, J.B. Cross, V. Bakken, C. Adamo, J. Jaramillo, R. Gomperts, R.E. Stratmann, O. Yazyev, A.J. Austin, R. Cammi, C. Pomelli, J.W. Ochterski, R.L. Martin, K. Morokuma, V.G. Zakrzewski, G.A. Voth, P. Salvador, J.J. Dannenberg, S. Dapprich, A.D. Daniels, O. Farkas, J.B. Foresman, J.V. Ortiz, J. Cioslowski and D.J. Fox, Gaussian 09, Revision D.01, Gaussian Inc., Wallingford (CT) (2013).
12. R. Dennington, T. Keith and J. Millam, Semichem Inc., Shawnee Mission, Gaussview 6 (2016).
13. R. Krishnan, J.S. Binkley, R. Seeger and J.A. Pople, *J. Chem. Phys.*, **72**, 650 (1980); https://doi.org/10.1063/1.438955
14. M.H. Jamróz, *Spectrochim. Acta A Mol. Biomol. Spectrosc.*, **114**, 220 (2013); https://doi.org/10.1016/j.saa.2013.05.096
15. M.P. Andersson and P. Uvdal, *J. Phys. Chem. A*, **109**, 2937 (2005); https://doi.org/10.1021/jp045733a
16. Chemcraft - Graphical Software for Visualization of Quantum Chemistry Computations, Version 1.8, build 682; https://www.chemcraftprog.com
17. J.E. Carpenter and F. Weinhold, *J. Mol. Struct. THEOCHEM*, **169**, 41 (1988); https://doi.org/10.1016/0166-1280(88)80248-3
18. T. Lu and F. Chen, *J. Comput. Chem.*, **33**, 580 (2012); https://doi.org/10.1002/jcc.22885
19. A. Daina, O. Michielin and V. Zoete, *Sci. Rep.*, **7**, 42717 (2017); https://doi.org/10.1038/srep42717
20. D. Schneidman-Duhovny, Y. Inbar, R. Nussinov and H.J. Wolfson, *Nucleic Acids Res.*, **33(Web Server)**, W363 (2005); https://doi.org/10.1093/nar/gki481
21. Z. Gabelica, *Spectrochim. Acta A*, **32**, 327 (1976); https://doi.org/10.1016/0584-8539(76)80085-2
22. R.L. Pecsok, Modern Methods of Chemical Analysis, Wiley, edn. 2 (1976).
23. P. Manikandan, M. Kumar, P. Swarnamughi, M. Asif, M. Nasibullah, V.S. Jeba Reeda, J.M. Khaled and S. Muthu, *J. Mol. Liq.*, **405**, 125064 (2024); https://doi.org/10.1016/j.molliq.2024.125064
24. A. McIlroy and D.J. Nesbitt, *J. Chem. Phys.*, **91**, 104 (1989); https://doi.org/10.1063/1.457496
25. L. Kahovec and K.W.F. Kohlrausch, *Monatsh. Chem.*, **74**, 333 (1941); https://doi.org/10.1007/BF01512909
26. M. Orozco and F.J. Luque, Generalization of the Molecular Electrostatic Potential for the Study of Noncovalent interactions. In: Theoretical and Computational Chemistry, Elsevier, vol. 3, pp. 181–218 (1996).
27. P. Manikandan, M. Kumar, S. Kaleeswaran, S. Chithra, P. Swarnamughi, M. Nikpassand and J.U. Prakash, *J. Indian Chem. Soc.*, **102**, 101657 (2025); https://doi.org/10.1016/j.jics.2025.101657
28. J.P. Foster and F. Weinhold, *J. Am. Chem. Soc.*, **102**, 7211 (1980); https://doi.org/10.1021/ja00544a007
29. K. Arulaabaranam, S. Muthu, G. Mani and A. Irfan, *J. Mol. Liq.*, **341**, 116934 (2021); https://doi.org/10.1016/j.molliq.2021.116934
30. B. Silvi and A. Savin, *Nature*, **371**, 683 (1994); https://doi.org/10.1038/371683a0
31. V.S. Jeba Reeda, J.N. CheerlinMishma, P. Divya, A. Manikandan, R. Suja, M. Shahid, H. Arora, A. Ali, N. Siddiqui and S. Javed, *Spectrosc. Lett.*, **0**, 1 (2024); https://doi.org/10.1080/00387010.2024.2401990
32. N. Elangovan, R. Sangeetha, S. Sowrirajan, S. Sarala and S. Muthu, *Anal. Chem. Lett.*, **12**, 58 (2022); https://doi.org/10.1080/22297928.2021.1933588
33. T. Lu and Q. Chen, *Chem. Methods*, **1**, 231 (2021); https://doi.org/10.1002/cmtd.202100007
34. X.D. Divya Dexlin, J.D. Deephlin Tarika, M. Sethuram and T. Joselin Beaula, *J. Mol. Liq.*, **351**, 118687 (2022); https://doi.org/10.1016/j.molliq.2022.118687
35. J.J. Kores, I.A. Danish, T. Sasitha, J.G. Stuart, E.J. Pushpam and J.W. Jebaraj, *Heliyon*, **7**, e08377 (2021); https://doi.org/10.1016/j.heliyon.2021.e08377
36. N. Issaoui, H. Ghalla, F. Bardak, M. Karabacak, N. Aouled Dlala, H.T. Flakus and B. Oujia, *J. Mol. Struct.*, **1130**, 659 (2017); https://doi.org/10.1016/j.molstruc.2016.11.019
37. A.D. Isravel, J.K. Jeyaraj, S. Thangasamy and W.J. John, *Comput. Theor. Chem.*, **1202**, 113296 (2021); https://doi.org/10.1016/j.comptc.2021.113296
38. D.A. Filimonov, A.A. Lagunin, T.A. Gloriozova, A.V. Rudik, D.S. Druzhilovskii, P.V. Pogodin and V.V. Poroikov, *Chem. Heterocycl. Compd.*, **50**, 444 (2014); https://doi.org/10.1007/s10593-014-1496-1
39. G.N. Ramachandran and V. Sasisekharan, Conformation of Polypeptides and Proteins, In: Advances in Protein Chemistry, Elsevier, vol. 23, pp. 283–437 (1968).
40. D.F. Veber, S.R. Johnson, H.-Y. Cheng, B.R. Smith, K.W. Ward and K.D. Kopple, *J. Med. Chem.*, **45**, 2615 (2002); https://doi.org/10.1021/jm020017n
41. C.A. Lipinski, *J. Pharmacol. Toxicol. Methods*, **44**, 235 (2000); https://doi.org/10.1016/S1056-8719(00)00107-6
42. J.R. Proudfoot, *Bioorg. Med. Chem. Lett.*, **12**, 1647 (2002); https://doi.org/10.1016/S0960-894X(02)00244-5
43. C. Zhang, G. Vasmatzis, J.L. Cornette and C. DeLisi, *J. Mol. Biol.*, **267**, 707 (1997); https://doi.org/10.1006/jmbi.1996.0859
44. H.M. Berman, T. Battistuz, W.F. Bluhm, P.E. Bourne, K. Burkhardt, T.N. Bhat, Z. Feng, G.L. Gilliland, L. Iype, S. Jain, P. Fagan, J. Marvin, D. Padilla, V. Ravichandran, B. Schneider, N. Thanki, H. Weissig, J.D. Westbrook and C. Zardecki, *Acta Cryst.*, **D58**, 899 (2002); https://doi.org/10.1107/S0907444902003451
45. M. Asif, M. Saquib, A. Rahman Khan, F. Aqil, A. salem Almalki, F. Ali Alasmary, J. Singh and M. Nasibullah, *ChemistrySelect*, **8**, e202204536 (2023); https://doi.org/10.1002/slct.202204536